Control Engineering Practice 68 (2017) 89–101

Contents lists available at ScienceDirect

Control Engineering Practice

journal homepage: www.elsevier.com/locate/conengprac

# Design and experimental validation of a physics-based oxygen storage — thermal model for three way catalyst including aging

Stefano Sabatini, Simone Gelmini, Mark A. Hoffman, Simona Onori *

*Department of Automotive Engineering - Clemson University, Clemson, SC 29607, USA*

A B S T R A C T

In this paper, a physics-based, oxygen storage-thermal model for a three way catalyst (TWC) is developed and experimentally validated. This model is then extended to account for aging impacts on the TWC. In order to identify the model parameters, a series of *ad hoc* experiments were designed to test the device over various engine operating conditions. Four TWCs of different ages were tested to investigate the effects of TWC aging on the oxygen storage dynamics. Results show that aging can be lumped within a single model parameter, referred to as *oxygen storage capacity*. Sensitivity analysis shows only negligible dependence of oxygen storage capacity on catalyst operating temperature. The comprehensive model is validated over real driving conditions for different catalyst ages. The developed model has the potential to enhance the design of optimization-control techniques for fuel consumption benefits and on-board diagnostics health measurement robustness.



## 1. Introduction

Tightening emissions standards and the 54.5 mpg fleet average fuel efficiency target on production vehicles by 2025 have spurred great interest in pursuing advanced control and optimization strategies to improve engine and aftertreatment systems performance (EPA, 2011). In order to meet new emissions regulation targets, the engine and the exhaust gas aftertreatment system are becoming increasingly complex through the introduction of technologies such as exhaust gas recirculation, particulate filters, etc.

For such complex systems, the *traditional* calibration approach based on open loop experimental maps has become impractical. The use of mathematical models to predict system and component behavior has become the preferred method to obtain increased performance, speed-up the control development process and reduce the calibration effort, Zhu, Wang, Sun, and Chen (2015). In modern Direct Injection (DI) engines, a Gasoline Particulate Filter (GPF) is added downstream of the TWC to limit particulate emissions. In this configuration, the TWC behavior influences the oxygen content and exhaust gas temperature flowing into the particulate filter, wielding influence over GPF soot regeneration events (Nicolin, Rose, Kunath, & Boger, 2015). Therefore, accurate prediction of TWC outlet oxygen concentration and temperature are crucial for estimation of GPF soot loading and regeneration.

Catalytic converters decrease toxic exhaust gas emissions by catalyzing a redox (oxidation or reduction) reaction. In particular, the TWC is used to simultaneously reduce nitrogen oxides ($NOx$), while and oxidize hydrocarbons (HC) and carbon monoxide (CO) are oxidized. Modern catalytic converters are capable of conversion efficiency (at steady state) approaching 100% when the normalized air–fuel ratio is controlled near stoichiometry, see Fig. 1.

The normalized air–fuel ratio is defined as:

$$\lambda = \frac{(A/F)_{actual}}{(A/F)_{stoich}} \tag{1}$$

where $(A/F)_{actual}$ is the actual air to fuel ratio and $(A/F)_{stoich}$ is the stoichiometric air–fuel ratio. With this formulation, when $\lambda < 1$, there is more fuel compared to the stoichiometric condition and the exhaust gas is said to be *rich*. When $\lambda > 1$ there is more air relative to the stoichiometric condition and the exhaust gas is referred to as *lean*.

Tailpipe emissions are highly affected by transient variations of the pre-catalyst air–fuel ratio that occur during real driving conditions. In order to compensate for transient $\lambda$ deviations from stoichiometry, cerium is added to the TWC system and it functions as an oxygen buffer thanks to its ability to store and release oxygen, Kim (1982).

TWC performance is also dependent on catalyst temperature: the chemical reactions occurring in the catalyst guarantee a satisfactory pollutant conversion efficiency only above a certain threshold, usually around 300 °C (Fig. 2).

Catalyst temperature and oxygen storage level cannot be directly measured with commercial sensors. A cost effective option to monitor these quantities is through the use of properly designed modeling tools.

A wealth of literature has been published on after-treatment modeling for both diesel and gasoline engines (e.g. Chen and Wang, 2014,

* Corresponding author.
*E-mail addresses:* ssabati@clemson.edu (S. Sabatini), sgelmin@clemson.edu (S. Gelmini), mhoffm4@clemson.edu (M.A. Hoffman), sonori@clemson.edu (S. Onori).

http://dx.doi.org/10.1016/j.conengprac.2017.07.007
Received 21 October 2016; Received in revised form 18 July 2017; Accepted 20 July 2017
Available online 9 September 2017
0967-0661/

**Nomenclature**

| | |
|---|---|
| TWC | Three Way Catalyst |
| PSO | Particle Swarm Optimization |
| PDE | Partial Differential Equation |
| $t$ | Time [s] |
| $\lambda$ | Normalized air–fuel ratio |
| $T_{cat}$ | TWC solid phase temperature [K] |
| $T_g$ | TWC gas phase temperature [K] |
| $T_{amb}$ | External environment temperature [K] |
| $T_{exh}$ | Exhaust gas temperature [K] |
| $T_{lo}$ | Catalyst light off temperature [K] |
| $\dot{m}_{exh}$ | Exhaust gas mass flow rate [kg $s^{-1}$] |
| $\rho_g$ | Exhaust gas density [kg $m^{-3}$] |
| $\rho_s$ | TWC solid phase density [kg $m^{-3}$] |
| $c_{p_g}$ | Specific heat of the exhaust gas [J $kg^{-1}$ $K^{-1}$] |
| $c_s$ | TWC solid phase specific heat [J $kg^{-1}$ $K^{-1}$] |
| $\lambda_g$ | Exhaust gas conductivity [W $m^{-1}$ $K^{-1}$] |
| $\lambda_s$ | TWC solid phase conductivity [W $m^{-1}$ $K^{-1}$] |
| $h$ | Convective heat transfer coefficient [W $m^{-2}$ $K^{-1}$] |
| $h_{out}$ | Convective heat transfer coefficient with the environment [W $m^{-2}$ $K^{-1}$] |
| $\epsilon$ | TWC open cross sectional area [0 – 1] |
| $A_{cs}$ | TWC cross sectional area [$m^2$] |
| $A_{geo}$ | TWC specific geometric area [$m^{-1}$] |
| $A_{out}$ | TWC external surface [$m^2$] |
| $V_{cat}$ | TWC volume [$m^3$] |
| $D_{cat}$ | TWC diameter [m] |
| $z$ | Axial dimension [m] |
| $K_{reac}$ | Proportional constant of $\dot{Q}_{reac}$ [J $kg^{-1}$ $m^{-3}$] |
| $\Delta H_i$ | Reaction enthalpy difference [J $mol^{-1}$] |
| $i$ | Reaction index |
| $j$ | Computational cell index |
| $\dot{Q}_{reac}$ | Heat produced by reactions [W $m^{-3}$] |
| $\eta$ | TWC efficiency [0 – 1] |
| $R_i$ | Reaction rate for the $i$th reaction [mol $m^{-3}$ $s^{-1}$] |
| $k_i^f$ | Forward reaction rate ($i = 1, 2$) |
| $k_i^b$ | Backward reaction rate ($i = 1, 2$) |
| $K_i$ | Chemical equilibrium constant |
| $\Delta G_k$ | Gibbs free energy variation [J] |
| $OSC$ | Total Oxygen Storage Capacity [mol $m^{-3}$] |
| $u$ | Space velocity [m $s^{-1}$] |
| $k_{rad}$ | Radial mass transfer coefficient [m $s^{-1}$] |
| $c_0$ | Total concentration in the gas [mol $m^{-3}$] |
| $M_{exh}$ | Average molar mass of composition [kg $mol^{-1}$] |
| $E_i$ | Activation energy [J $mol^{-1}$] |
| $A_i$ | Pre-exponential factor |
| $\phi$ | Normalized oxygen storage level [0 – 1] |
| Ce | Cerium chemical element symbol |
| $[Y]$ | Concentration of species $Y$ [mol $m^{-3}$] |
| $[Y]_g$ | Concentration of species $Y$ in the gas [mol $m^{-3}$] |
| $[Y]_{wc}$ | Concentration of species $Y$ in the washcoat [mol $m^{-3}$] |

Depcik and Assanis, 2005, Guzzella and Onder, 2009, Katare, Patterson, and Laing, 2007 and Lepreux, Creff, and Petit, 2012). Despite the differences in the adopted technologies, the common modeling challenge lies in considering the complex mass transport, thermal and chemical dynamics typical of aftertreatment systems to predict, in a computationally efficient way, the macroscopic phenomena of interest.

Two modeling approaches are predominant in literature: physics-based modeling and empirical modeling. Physics-based models for TWC are developed in Auckenthaler (2005), Depcik and Assanis (2005), Montenegro and Onorati (2009), Oh and Cavendish (1982) and in Shamim,

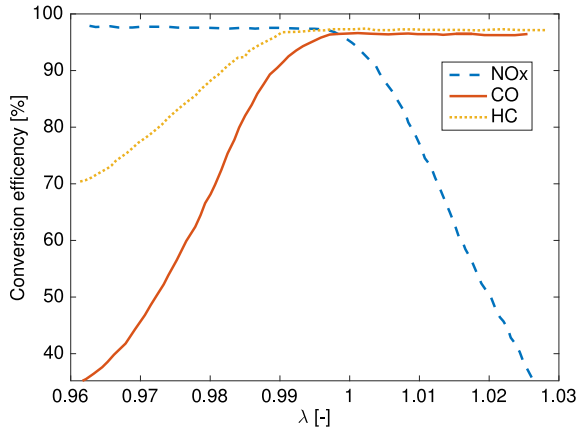


**Fig. 1.** Dependence of the TWC steady state conversion efficiency on the normalized air–fuel ratio $\lambda$.
*Source:* Figure reproduced from DTEC (2011).

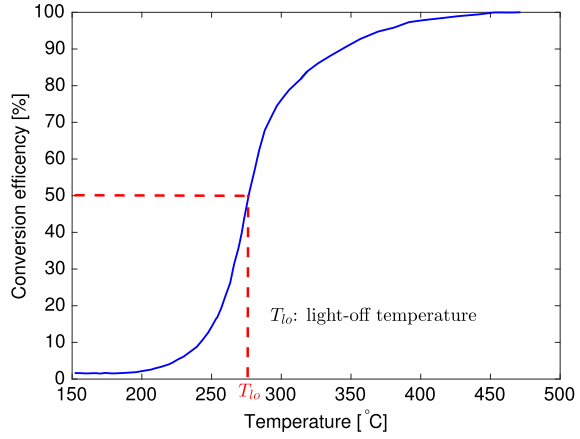


**Fig. 2.** The effect of temperature on TWC conversion efficiency, Bresch-Pietri, Leroy, and Petit (2013). The "light-off temperature" of the converter is defined as the temperature at which the reduction efficiency reaches 50%, Brandt, Wang, and Grizzle (2000).

Shen, Sengupta, Son, and Adamczyk (2002). In those works, the TWC operation is described using energy and mass balance equations coupled with a complex kinetics model to predict the conversion of undesired engine emission species within the catalyst. Estimation of the kinetic parameters can make identification of these models quite challenging. In addition, physics-based models are computationally complex, as they utilize non-linear coupled Partial Differential Equations (PDEs). The real time application of such models for temperature estimation and oxygen storage level control is highly limited.

In Kumar et al. (2012) and Möller, Votsmeier, Onder, Guzzella, and Gieshoff (2009), physic-based models are considered but with a reduced number of chemical species. Even though the computational burden of these models is reduced, their real-time application is still unfeasible since the chemical species concentrations at the catalyst inlet are required inputs and no gas analyzer is available for today's production vehicles. In Bickel, Odendall, Eigenberger, and Nieken (2017), a 1-D model with a simplified kinetic reaction is developed to study the oxygen storage capability of fresh catalysts under very different precious metal loadings. The resulting model was characterized using only five parameters. In Kiwitz, Onder, and Guzzella (2012), a simple physics-based oxygen storage model with a reduced number of species is presented, where the species concentrations are estimated from the wide-range lambda sensor measurements upstream the catalyst.

A large number of computationally tractable, semi-empirical models suitable for on-board control can be found in literature, such as, Balenovic (2002), Brandt et al. (2000), Cioffi, Scala, and Sepe (2001), Jones, Roberts, Bernard, and Jackson (2000) and Tomforde, Drewelow, Duenow, Lampe, and Schultalbers (2013). These models are referred to as *storage dominated models* and are based on the mass balance of oxygen. In different ways, they account for oxygen adsorption and release rate, using non-linear empirical functions of the actual oxygen storage level. Most storage dominated models neglect the dependence of oxygen storage dynamics on catalyst temperature and, because of their simplicity, do not guarantee a predefined accuracy over a wide range of operating conditions, especially during the warm up phase.

In this paper, the physics-based oxygen storage model from Kiwitz et al. (2012) is coupled with a PDE-based temperature model of the TWC and applied to a partial volume catalyst system consisting of two catalyst bricks. The parameters of both the temperature and oxygen storage models are identified utilizing experiments conducted across a wide range of engine operating conditions. The model is then validated over real driving cycles, demonstrating its ability to estimate the air–fuel ratio dynamics downstream of the catalyst.

The effects of age on TWC oxygen storage dynamics is investigated in this work through experimentation with catalysts of different ages. Insights are given on how the two catalyst bricks unevenly age during normal catalyst operation.

Compared to the semi-empirical models presented in literature, the proposed model better characterizes the effects of temperature and aging on the TWC oxygen storage dynamics, providing insights for designing more accurate on-board diagnostic algorithms. In contrast with higher order, physics-based models where a complete description of the chemical reactions occurring within the catalyst is required, the reduced order model presented herein is suitable for TWC estimation during real-time vehicle operation.

The paper is organized as follows. In Section 2, the TWC system is described and the requirements for a complete TWC control oriented model are highlighted. The governing equations for temperature and oxygen storage dynamics are derived in Section 3. In Sections 4 and 5, the experimental setup used for data collection and the procedure for model parameter identification are presented. In Section 6, the TWC aging study and the role of age in the proposed model are discussed. The model is validated over real driving scenarios in Section 7. Finally, conclusions are provided in Section 8.

## 2. Three way catalyst device

The catalytic converter is composed of a substrate, washcoat and a mix of precious metals (Fig. 3). The substrate usually consists of a honeycomb ceramic block through which the exhaust gas flows. The washcoat is the carrier for the catalytic material and is applied to the substrate in order to provide a porous layer that greatly increases the surface area. The catalytic material usually consists of precious metal mixture such as Platinum (Pt), Palladium (Pd) and Rhodium (Rh) that enables the conversion of the pollutants. Cerium is added to provide the oxygen storage capability.

Although large quantity of chemical processes are occurring in the TWC, the dynamic behavior of the converter is dominated by the oxygen storage capability of the cerium washcoat. This catalyst property is exploited as an oxygen buffer, which compensates for air–fuel ratio deviations from stoichiometry ($\lambda = 1$) to maximize pollutant conversion efficiency. When the engine is running lean ($\lambda > 1$), HC and CO are completely oxidized because of the excess oxygen in the exhaust gas. Oxygen is stored in the cerium until the oxygen storage capacity of the converter is saturated. However, once the oxygen storage capacity is saturated, NO$x$ reduction ceases. On the other hand, when the engine is running rich ($\lambda < 1$), there is inadequate exhaust gas oxygen to oxidize all the CO and HC. Therefore, the oxygen previously stored in the cerium is released to compensate for such a deficiency.

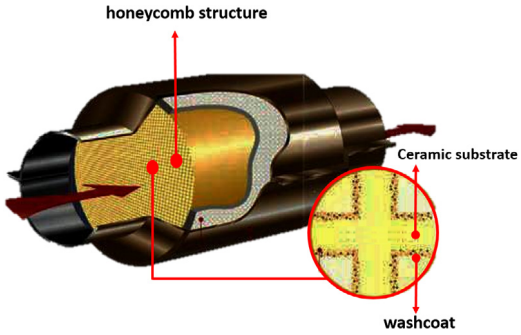


**Fig. 3.** TWC cutaway showing the internal honeycomb structure of the converter. *Source:* Figure reproduced from VSCHT (2011).

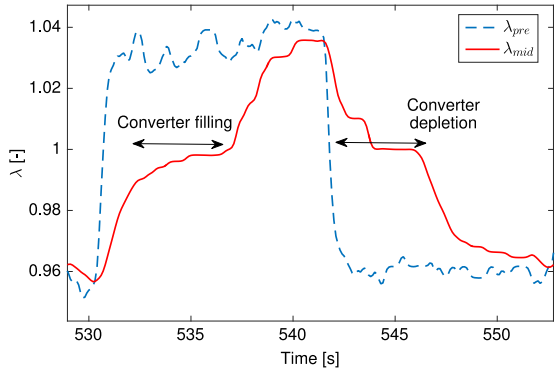


**Fig. 4.** Effect of the oxygen storage capability on lambda measurements: when an air–fuel ratio step change ($\lambda_{pre}$) is commanded upstream of the catalyst, the delayed downstream lambda sensor response ($\lambda_{mid}$) is an indication of oxygen storage activity in the catalyst.

The quantity of oxygen stored in the catalyst cannot be directly measured, but the TWC oxygen storage effect can be estimated by analyzing the response of sensors present in a modern vehicle after treatment system. Two lambda sensors are usually present in a partial volume configuration such as the sensor layout considered in this work. The first lambda sensor is located upstream of the TWC, and the second is positioned directly downstream of right after the first brick (see, Fig. 11). When a rich to lean air–fuel ratio step change is commanded, the excess oxygen in the exhaust gas is stored in the converter and the lambda sensor reads stoichiometry until the oxygen capacity is saturated. A similar behavior can be observed during the converter depletion phase when a lean to rich step change is commanded (Fig. 4).

Intuitively, it is preferable to maintain an intermediate oxygen storage level to allow the converter to compensate for both rich and lean air–fuel ratio deviations from stoichiometry and prevent pollutant breakthrough at the vehicle tailpipe. To achieve this goal, the oxygen storage level needs to be tracked during vehicle operation. The most practical and cost effective way to estimate the oxygen storage level is to use models relying on lambda sensors.

Another important factor that influences TWC performance is the temperature of the catalyst substrate, as shown in Fig. 2. Engine control strategies are specifically designed to minimize the TWC warm up time using the heat from the exhaust gas. Information about catalyst temperature can be useful to design a closed-loop control strategy focused on TWC warmup to minimize pollutant emissions and the fuel consumption during a cold start. Temperature not only influences the TWC steady state conversion efficiency, but it also affects its oxygen storage dynamics. In fact, catalyst temperature affects the reaction rates occurring in the TWC and consequently the oxygen adsorption and release rates.

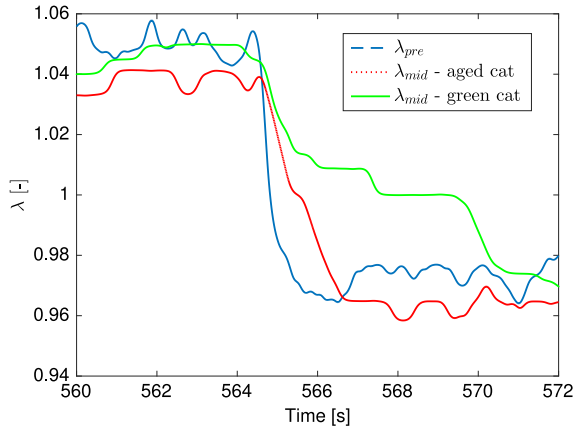


**Fig. 5.** Effect of aging on the oxygen storage dynamics.

Catalyst performance decreases over time due to chemical and/or thermal mechanisms causing the catalyst to age. One of the most relevant aging effects is the degradation of the converter's oxygen storage capability. This fact can be appreciated from Fig. 5 where the lambda response at the mid-catalyst location to an air–fuel ratio step change is shown for a fresh and a strongly aged catalyst. The oxygen depletion phase is substantially shorter for the aged catalyst, suggesting that an aged catalyst stores only a fraction of the oxygen that is stored in a fresh catalyst. This behavior must be accounted for in developing a control oriented TWC model since the normalized oxygen storage level estimation is ultimately dependent on the maximum quantity of oxygen that can be stored in the converter.

## 3. Three way catalyst model

TWC behavior can be described by a system of nonlinear PDEs derived from the conservation of the mass, energy and chemical species within the converter. The governing equations can be found in Shamim et al. (2002) along with complete kinetic models describing the different reaction paths occurring in the catalyst. Models proposed in Shamim et al. (2002) account for more than 20 reactions and are able to predict the TWC conversion efficiency. However, this level of detail is too complex for real-time estimation and control. As discussed in the previous section, from a control perspective, it is sufficient to model the TWC oxygen storage capability and the converter temperature dynamics. In this work, a detailed thermal model is derived in Section 3.1 and the oxygen storage model in Section 3.2.

### 3.1. Thermal model

The TWC temperature models found in the literature are mostly used for real-time estimation. Brandt et al. (2000) use the estimated brick temperature as an input to a static catalyst conversion efficiency map in order to predict CO, NO and HC emissions. In Cioffi et al. (2001), the adsorption rate of an empirical oxygen storage model depends on temperature estimation. In both cases, the temperature model is a first order ODE whose parameters are empirically identified. Given that the above approaches model the converter as a lumped system, they lack accurate of predictability over a wide range of operating conditions.

In Bresch-Pietri et al. (2013), a control-oriented TWC temperature model is obtained by simplifying the partial differential equations describing the energy balance into a time-varying input delay model. In that work, TWC inlet concentrations of CO, $NO_x$ and HC are model inputs for reaction heat characterization. Species measurement concentrations are not available in production vehicles. Thus the model is not suitable for real time operation. In the temperature model presented here, the heat produced by chemical reactions is lumped in a single term so that the species concentrations are not needed as model inputs.

Following the one dimensional approach, Shamim et al. (2002), the TWC thermal behavior can be described by performing an energy balance on the exhaust gas and another energy balance on the TWC solid phase representing the substrate and the washcoat lumped together. The two equations are:

**Energy balance in the gas phase:**

$$\rho_g \epsilon c_{p_g} \frac{\partial T_g}{\partial t} = -\frac{\dot{m}_{exh}}{A_{cs}} c_{p_g} \frac{\partial T_g}{\partial z} + hA_{geo}(T_{cat} - T_g). \tag{2}$$

**Energy balance in the solid phase:**

$$\begin{aligned} \rho_s(1-\epsilon)c_s \frac{\partial T_{cat}}{\partial t} &= (1-\epsilon)\lambda_s \frac{\partial^2 T_{cat}}{\partial z^2} - hA_{geo}(T_{cat} - T_g) \\ &\quad + \textstyle\sum_i(-\Delta H_i R_i) - \frac{A_{out}}{V_{cat}} h_{out}(T_{cat} - T_{amb}). \end{aligned} \tag{3}$$

The physical meaning of each symbol is explained in the Nomenclature. The first term on the right hand side of Eq. (2) represents the heat flow along the TWC axis due to the flow of the exhaust gas and the term $hA_{geo}(T_{cat} - T_g)$ in (2) and (3) accounts for the heat exchange between the gas and the catalyst. In (3), the term $\frac{A_{out}}{V_{cat}} h_{out}(T_{cat} - T_{amb})$ accounts for the convective losses to the ambient and the terms $(1-\epsilon)\lambda s \frac{\partial^2 T_{cat}}{\partial z^2}$ and $hA_{geo}(T_{cat} - T_g)$ account for conduction and convection between gas and substrate, $t$ produced by the exothermic reactions occurring in the washcoat where $R_i$ stands for the rate of $i$th respectively. The term $\sum_i(-\Delta H_i R_i)$ represents the heat generated by the chemical reactions, where $R_i$ is the rate of i-th reaction.

Some simplifications are made to (2)–(3): first, given that gas temperature dynamics are much faster than the catalyst temperature dynamics, the storage term in (2) can be neglected, leaving $T_g$ at steady state. Furthermore, previous studies (Montenegro & Onorati, 2009) have shown that the convective heat exchange and the heat from exothermic reactions are the dominant factors in the substrate energy balance (3) during normal catalyst operation. Thus, the term $(1-\epsilon)\lambda_s \frac{\partial^2 T_{cat}}{\partial z^2}$ in Eq. (3), representing the conduction along the substrate is neglected due to the low conductivity of the substrate material (cordierite). The heat loss to the ambient becomes relevant at high temperatures and therefore retained.

To fully describe the heat produced by the chemical reactions, a complete kinetic model would be needed to determine reaction rates $R_k$. This would lead to a complex and computationally expensive model not suitable for control purposes. Furthermore the development of a kinetic model requires quantitative information about inlet species concentrations, which is not available in current productions vehicles. Therefore, the heat produced by the chemical reactions is lumped into a single term $\dot{Q}_{reac}$. This term is related to the catalyst efficiency and dominates the energy balance after light-off while it is close to zero for temperatures below the catalyst light-off. Furthermore $\dot{Q}_{reac}$ is considered proportional to the exhaust mass flow rate $\dot{m}_{exh}$ and no dependence on inlet species concentration is considered.

$$\dot{Q}_{reac} = K_{reac} \dot{m}_{exh} \eta(T_{cat}). \tag{4}$$

This assumption is accurate as long as the catalyst operates around stoichiometric conditions where the majority of the hydrocarbons and carbon-monoxide are oxidized and therefore, the exothermic contribution depends only on the flow rate of the incoming pollutants. This is assured by today's air–fuel ratio controls which command an oscillating pre-TWC lambda very close to stoichiometry. If the catalyst experiences extended operation in either severely lean or severely rich conditions, the reaction heat model is not expected to be accurate. The TWC conversion efficiency has been chosen to be a hyperbolic function of the catalyst temperature so to reproduce the S-shaped efficiency behavior, as presented in Kang et al. (2014):

$$\eta(T_{cat}) = 0.5 \tanh(a(T_{cat} - T_{light\text{-}off})) + 0.5 \tag{5}$$

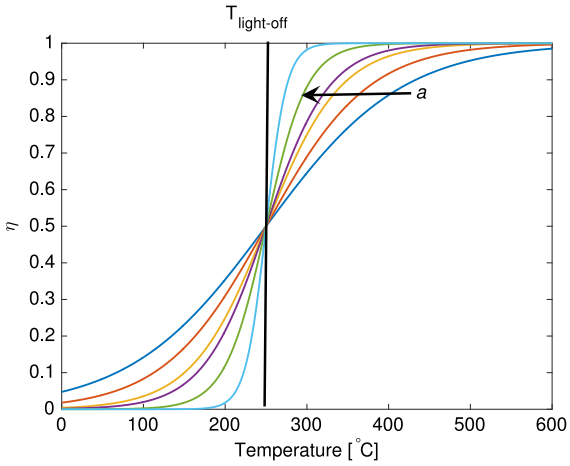


**Fig. 6.** S-shaped efficiency curve for TWC.

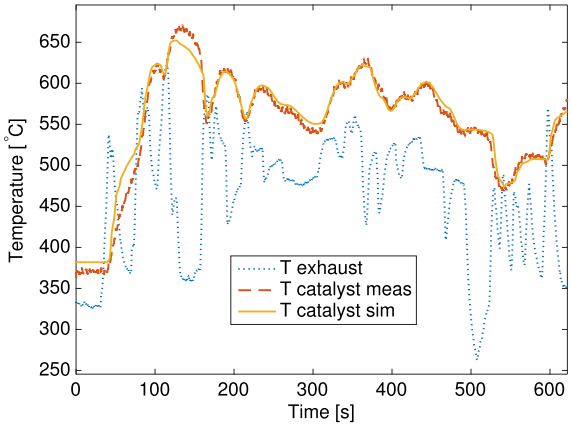


**Fig. 7.** Temperature model performance on FUDS.

where $a$ is a parameter describing the slope of the efficiency curve while $T_{light\text{-}off}$ represents the catalyst light off temperature (Fig. 6). In conclusion the PDEs (2) and (3) are simplified as follow:

$$\frac{\dot{m}_{exh}}{A_{cs}} c_{p_g} \frac{\partial T_g}{\partial z} = hA_{geo}(T_{cat} - T_g) \tag{6}$$

$$\rho_s(1-\epsilon)c_s \frac{\partial T_{cat}}{\partial t} = -hA_{geo}(T_{cat} - T_g) + \dot{Q}_{reac} - \frac{4}{D_{cat}} h_{out}(T_{cat} - T_{amb}). \tag{7}$$

The boundary and initial conditions are:

$$\begin{aligned} T_g(t) \quad \Big|_{z=0} &= T_{exh}(t) \\ T_{cat}(z) \quad \Big|_{t=0} &= T_{cat_0}(z). \end{aligned} \tag{8}$$

In Eqs. (6) and (7), the parameters $\rho_s c_s$, $h$ and $h_{out}$ are related to the thermal properties of the TWC materials, which are not perfectly known a priori. Furthermore, the lumped reaction heat generation is parametrized through $T_{light\text{-}off}$, $a$ and $K_{reac}$ which are to be identified. The identification of these parameters is performed through specific experimental tests, as described in Sabatini et al. (2015). The model is validated over real driving conditions (Federal Urban Driving Cycle) and the results are shown in Fig. 7.

### 3.2. Oxygen storage model

The air–fuel ratio at the TWC inlet should be regulated to minimize CO, $NO_x$ and HC emissions. Accurate estimation within the catalytic converter would require a complex model, which would be impractical for both identification and real-world implementation. On the other hand, an indirect method for TWC emissions control is through controlling the TWC oxygen storage level such that the transient deviation of the air–fuel ratio can be overcome by the cerium's capability to store and release oxygen. For this reason, the oxygen storage model presented in Kiwitz et al. (2012) considers only the chemical species involved in oxygen storage. During normal engine operating conditions, the HC concentration in the exhaust gas is negligible compared to the CO concentration. $NO_x$ concentration is also small compared to $O_2$ therefore only $O_2$, is considered, Auckenthaler (2005).

The reaction scheme consists of two reactions following the Eley–Rideal mechanism:

$$O_2 + 2Ce_2O_3 \longleftrightarrow 2Ce_2O_4 \tag{9a}$$

$$CO + Ce_2O_4 \longleftrightarrow CO_2 + Ce_2O_3. \tag{9b}$$

The first reaction (9a) accounts for the oxygen adsorption on the catalyst surface, while the second reaction (9b) accounts for the CO oxidation with the oxygen previously adsorbed on the catalyst.

Both the forward and backward reactions, respectively, described by (9a) and (9b), are taken into account resulting in the following net reaction rates:

$$R_1 = k_1^f [Ce_2O_3]^2[O_2] - k_1^b [Ce_2O_4]^2 c_0 \tag{10a}$$

$$R_2 = k_2^f [Ce_2O_4][CO] - k_2^b [Ce_2O_3][CO_2] \tag{10b}$$

where, $[Y]$ indicates the concentration of the chemical species $Y$, with $Y = O_2$, CO, $CO_2$, Ce, CeO, and $c_0 = \frac{P}{RT_g}$ is the total exhaust gas concentration. For clarity, note that the squared dependence of the forward and backward reaction rates in Eq. (10a) correlates to the need for two Ceria sites to complete reaction Eq. (9a).

Forward reaction rate $k_i^f$ (with $i = 1, 2$), conforming to reaction rate of Eqs. (10a) and (10b), depends on temperature through the Arrhenius type equation:

$$k_i^f = A_i e^{-\frac{E_i}{RT_{cat}}}. \tag{11}$$

The backward reaction constant is linked to the forward reaction constant through the chemical equilibrium constant $K_i$ which is a function of the Gibbs energy change $\Delta G$ of each reaction:

$$\begin{aligned} k_i^b &= \frac{k_i^f}{K_i} \\ K_i &= e^{-\frac{\Delta G_i}{RT_{cat}}}. \end{aligned} \tag{12}$$

$$\frac{\Delta G_1}{RT_{cat}} \approx \frac{2\left(a_{Ce_2O_4} T_{cat} + b_{Ce_2O_4}\right)}{T_{cat} + c_{Ce_2O_4}} + -\frac{a_{O_2} T_{cat} + b_{O_2}}{T_{cat} + c_{O_2}} \tag{13a}$$

$$\frac{\Delta G_2}{RT_{cat}} \approx \frac{a_{Ce_2O_4} T_{cat} + b_{Ce_2O_4}}{T_{cat} + c_{Ce_2O_4}} + -\frac{a_{CO_2} T_{cat} + b_{CO_2}}{T_{cat} + c_{CO_2}} + \frac{a_{CO} T_{cat} + b_{CO}}{T_{cat} + c_{CO}}. \tag{13b}$$

The parameters $a_Y$; $b_Y$; $c_Y$ in (13a) and (13b) - where the subscript $Y$ indicates the chemical species involved in the reaction - are identified over experimental data. The oxidized and empty surface sites sum to the total oxygen storage capacity OSC (in $mol/m^3$):

$$[Ce_2O_3] + [Ce_2O_4] = OSC. \tag{14}$$

The species concentration dynamics along the catalyst length are typically described through two concentration balances: one in the exhaust gas, and another in the washcoat where the chemical reactions occur. According to Shamim et al. (2002), the equations are:

**Concentration balance in the gas phase**:

$$\epsilon \frac{\partial [Y]_g}{\partial t} = -u \frac{\partial [Y]_g}{\partial z} - k_{rad} A_{geo}([Y]_g - [Y]_{wc}). \tag{15}$$

**Concentration balance in the washcoat**:

$$(1-\epsilon)\frac{\partial [Y]_{wc}}{\partial t} = k_{rad} A_{geo}([Y]_g - [Y]_{wc}) - R_k. \tag{16}$$

In the kinetic model above, $Y = O_2$, CO, $CO_2$ represents the relevant exhaust gas species (one PDE per species). The term $u\frac{\partial [Y]_g}{\partial z}$ accounts for the mass transport of each chemical species $Y$ along the catalyst axis, the term $k_{rad}A_{geo}([Y]_g - [Y]_{wc})$ accounts for radial mass transport from the gas to the washcoat, and $R_Y$ is the net consumption rate for each chemical species $Y$.

In Eqs. (15) and (16), the radial mass transport is assumed to be fast, therefore negligible. Under this assumption, the gas phase and the washcoat are lumped together and the concentration balances can be written as:

$$\begin{aligned}
\frac{\partial [O_2]}{\partial t} &= -u\frac{\partial [O_2]}{\partial z} - R_1 \\
\frac{\partial [CO]}{\partial t} &= -u\frac{\partial [CO]}{\partial z} - R_2 \\
\frac{\partial [CO_2]}{\partial t} &= -u\frac{\partial [CO_2]}{\partial z} + R_2
\end{aligned} \tag{17}$$

where the space velocity, $u$, in first approximation can be rewritten as a function of the exhaust mass flow rate $\dot{m}_{exh}$:

$$u = \frac{\dot{m}_{exh}}{\rho_g A_{cs}} = \frac{\dot{m}_{exh}}{c_0 M_{exh} A_{cs}}. \tag{18}$$

Since the exhaust gas dynamics are much faster than the oxygen storage dynamics (Depcik & Assanis, 2005), the storage term can be neglected and (17) can be rewritten as:

$$\begin{aligned}
\frac{\partial [O_2]}{\partial z} &= -R_1 \frac{c_0 M_{exh} A_{cs}}{\dot{m}_{exh}} \\
\frac{\partial [CO]}{\partial z} &= -R_2 \frac{c_0 M_{exh} A_{cs}}{\dot{m}_{exh}} \\
\frac{\partial [CO_2]}{\partial z} &= +R_2 \frac{c_0 M_{exh} A_{cs}}{\dot{m}_{exh}}.
\end{aligned} \tag{19}$$

The quantity of oxygen stored in the TWC can be calculated considering the rates of oxygen adsorbed in and released from the cerium:

$$\frac{\partial \phi}{\partial t} = \frac{1}{OSC}(2R_1 - R_2) \tag{20}$$

where $\phi$ represents the oxygen storage level normalized with respect to total oxygen storage capacity, $OSC$. Because the reaction of Eq. (9a) simultaneously involves two cerium sites, the level of stored oxygen is sensitive to twice the reaction rate $R_1$.

In order to solve Eq. (19), the exhaust gas composition at the catalyst inlet must be specified. Since the model takes into account a reduced number of chemical species, the gas composition can be fully derived from the lambda measurement upstream of the catalyst with a few assumptions. In Guzzella and Onder (2009), the gas inlet composition is specified for the stoichiometric condition and gas compositions for other air–fuel ratios are derived from the lambda definition presented in Auckenthaler (2005). The fact that exhaust species concentrations are calculated only relying on the lambda sensor is an important feature of the model, avoiding the use of gas analyzers that are not present in production vehicles. The inlet concentrations as a function of lambda are summarized in Fig. 8. For further information about the model the reader is directed to Kiwitz et al. (2012).

### 3.3. Combined model and numerical solution

The thermal model described in Section 3.1 requires exhaust temperature $T_{exh}$ and exhaust mass flow rate $\dot{m}_{exh}$ as inputs and provides an estimation of the catalyst temperature. The TWC temperature dynamics are decoupled from the chemical kinetics, lumping the heat produced by the exothermic reactions in the single term $\dot{Q}_{reac}$ that does not depend on the inlet species concentration (see, Eq. (4)). The oxygen storage model takes into account only two reactions and the exhaust gas composition

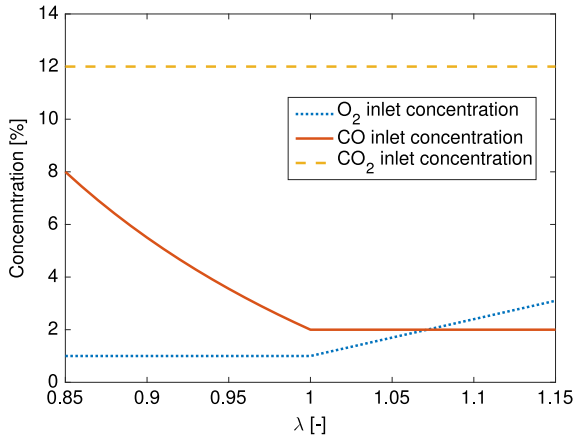


**Fig. 8.** Inlet species concentrations as a function of lambda.

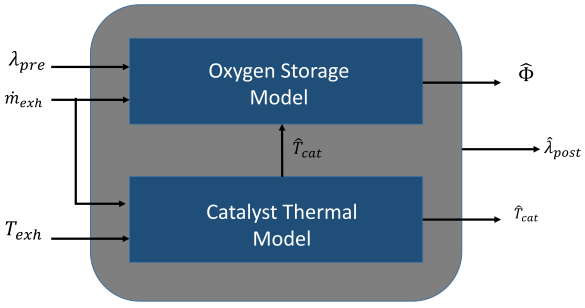


**Fig. 9.** Structure of the proposed TWC model.

is derived from the upstream lambda sensor measurement. The two reaction rates $R_1$ and $R_2$, depend on catalyst temperature. Therefore, the estimation performed by the thermal model is an input to the oxygen storage model. A schematic of the TWC model developed in this paper is shown in Fig. 9.

For numerical simulations, (6), (7), (19) and (20) need to be spatially discretized. The discretization has been performed using a finite difference upwind scheme, substituting the general spatial derivative $\frac{df(z)}{dz}$ with $\frac{f^j - f^{j-1}}{\Delta z}$ where $j$ is the $j$th computational cell and $\Delta z$ is the spatial discretization step (LeVeque, 2007). After the discretization and some algebraic manipulations, the model equations result in:

**Thermal model:**

$$\begin{aligned}
T_g^j &= \frac{T_g^{j-1} + \frac{hA_{geo}A_{cs}\Delta z}{\dot{m}_{exh}c_{p_g}} T_{cat}^j}{1 + \frac{hA_{geo}A_{cs}\Delta z}{\dot{m}_{exh}c_{p_g}}} \\
\frac{dT_{cat}^j}{dt} &= -\frac{hA_{geo}}{\rho_s(1-\epsilon)c_s}(T_{cat}^j - T_g^j) + \frac{\dot{Q}_{reac}}{\rho_s(1-\epsilon)c_s} - \frac{4h_{out}(T_{cat}^j - T_{amb})}{D_{cat}\rho_s(1-\epsilon)c_s}.
\end{aligned} \tag{21}$$

**Oxygen storage model:**

$$\begin{aligned}
[O_2]^j &= [O_2]^{j-1} - R_1^j \cdot \frac{\Delta z c_0 M_{exh} A_{cs}}{\dot{m}_{exh}} \\
[CO]^j &= [CO]^{j-1} - R_2^j \cdot \frac{\Delta z c_0 M_{exh} A_{cs}}{\dot{m}_{exh}} \\
[CO_2]^j &= [CO_2]^{j-1} + R_2^j \cdot \frac{\Delta z c_0 M_{exh} A_{cs}}{\dot{m}_{exh}} \\
\frac{d\phi^j}{dt} &= \frac{1}{OSC} \cdot (2R_1^j - R_2^j).
\end{aligned} \tag{22}$$

The discretized model scheme is shown in Fig. 10.

For real time applications, an explicit, fixed step solver needs to be used. For this reason, Eqs. (22) and (21) have been integrated using the forward Euler method with a fixed time step of 0.01 s. A sensitivity

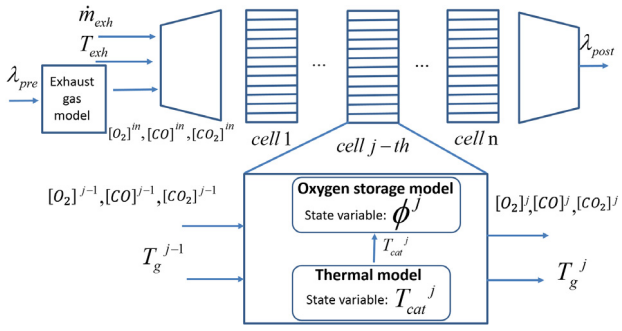


**Fig. 10.** TWC discretized modeling scheme. The model inputs are: lambda upstream of the catalyst ($\lambda_{pre}$), exhaust mass flow rate ($\dot{m}_{exh}$), and exhaust temperature ($T_{exh}$). These inputs can be either measured by commercially available sensors (oxygen sensors, air mass flow meters, thermocouples) or easily estimated by the ECU.

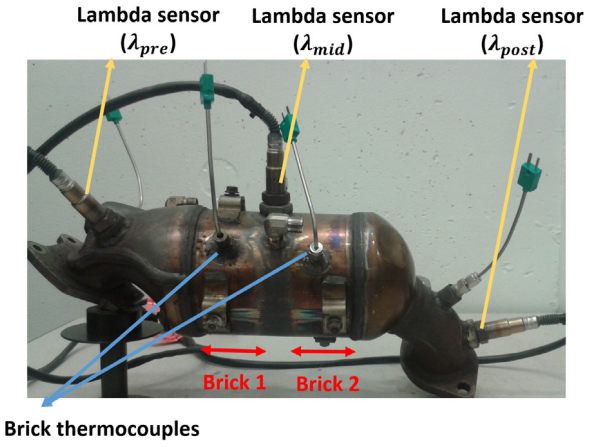


**Fig. 11.** Instrumented two-brick TWC used in this study.

**Table 1**
Catalyst specifications.

| | Brick 1 | Brick 2 |
|---|---|---|
| Length [mm] | 68 | 68 |
| Volume [l] | 0.597 | 0.597 |
| Cell density [cell/in$^2$] | 600 | 400 |

**Table 2**
Summary of the catalyst history (see Sabatini et al., 2016).

| | Aging process (equivalent mileage) | |
|---|---|---|
| | Brick 1 | Brick 2 |
| Green | –(0) | –(0) |
| Stock | On-road driving (20 k miles) | On-road driving (20 k miles) |
| Mid-life | Engine dyno (50 k miles) | Thermal aging cycle (50 k miles) |
| OBD | OBD aged (>150 k miles) | Thermal aging cycle (150 k miles) |

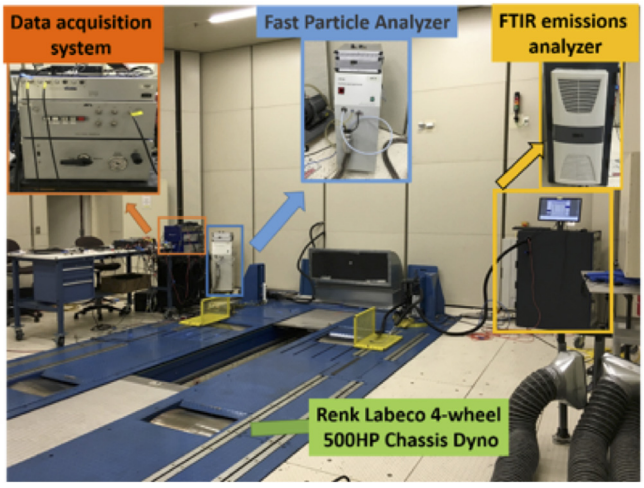


**Fig. 12.** Chassis dynamometer test cell (Renk Labeco 4-wheel, 500HP Chassis Dyno) with specialized emission analyzers and data acquisition system (Sabatini et al., 2016).

study with respect to the number of computational cells is presented in Section 5.2 along with the identification of the model parameters.

## 4. Experimental setup

The TWC used in this work is a close-coupled catalyst in a partial-volume monitoring configuration. In this configuration the converter consists of two catalyst monoliths (also called bricks) separated by a small gap and mounted within the same metal housing. Fig. 11 shows the TWC used in this work: the catalyst was instrumented with three wide range lambda sensors: the first is mounted upstream of the converter ($\lambda_{pre}$) the second sensor is placed between the two bricks ($\lambda_{mid}$) and the third is mounted downstream of the converter ($\lambda_{post}$). Thermocouples were also mounted at each of these locations to monitor the gas temperature, ($T_{exh}$, $T_{mid}$, $T_{post}$). One thermocouple is also installed in each catalyst monolith 1.5 in from the front face of the brick and penetrating to the flow centerline to measure the substrate temperatures. These sensors are used to identify the parameters and validate the performance of the thermal model presented in Section 3.1 ($T_{cat_1}$, $T_{cat_2}$). Most of these sensors are used only for parameter identification and monitoring purposes. The model developed here relies on physical measurements $\lambda_{pre}$, $T_{exh}$ and on the estimation of the exhaust flow rate $\dot{m}_{exh}$ performed by the ECU. Table 1 lists the specifications for the two catalyst bricks are listed.

Catalysts of various ages were used in this work to study how the model parameters must be adapted to account for converter aging. Four different catalysts were available: a Green catalyst, a so-called "Stock" catalyst aged through 20,000 miles of on-road driving, a Mid-Life catalyst and an OBD aged catalyst. The catalysts aging processes for both brick 1 and brick 2 are summarized in Table 2.

Tests for parameter identification and model validation were performed in a chassis dynamometer test cell (Renk Labeco 4-wheel, 500HP Chassis Dyno) at the Clemson University International Center for Automotive Research shown in Fig. 12.

## 5. Model identification

The model parameters identified for the oxygen storage model are summarized in Table 3. $A_1$, $A_2$ are the pre-exponential factors and $E_1$, $E_2$ the activation energies in Eq. (11). Parameters $a$, $b$, $c$ describe the Gibbs energy of the oxidized catalyst surface $G_{Ce_2O_4}$ as function of the catalyst temperature. The Gibbs energy of the other chemical species within the reaction scheme described by Eq. (9) retain the parameters used by Kiwitz et al. (2012). Since the first and second TWC bricks have different cell densities and precious metal loadings, a separate parameter set has been identified for each brick. In addition to the parameters in Table 3, the total oxygen storage capacity $OSC$, defined in Eq. (14), must be identified for each brick.

Since many different oxidation and reduction paths are lumped in the simple reaction scheme of Eq. (9), experiments designed to excite only certain reaction paths and identify each parameter separately are impractical. Instead a single experiment able to excite the oxygen storage dynamic is designed. The parameters are then identified simultaneously by analyzing the converter response. Furthermore, since production vehicles utilize only lambda sensors for control and diagnostics, the experimental design and the identification procedures focus on lambda sensor responses.

**Table 3**
Model parameters and their identified values.

| Parameter | Identified value | |
|---|---|---|
| | Brick 1 | Brick 2 |
| $A_1$ | $3.2 \cdot 10^3$ | $4.6 \cdot 10^3$ |
| $A_2$ | $2.4 \cdot 10^2$ | $1.7 \cdot 10^2$ |
| $E_1$ | $4.43 \cdot 10^4$ | $5.10 \cdot 10^4$ |
| $E_2$ | $3.59 \cdot 10^3$ | $5.82 \cdot 10^3$ |
| $a$ | 3.57 | 3.17 |
| $b$ | $-3.49 \cdot 10^4$ | $-3.42 \cdot 10^4$ |
| $c$ | 0 | 0 |

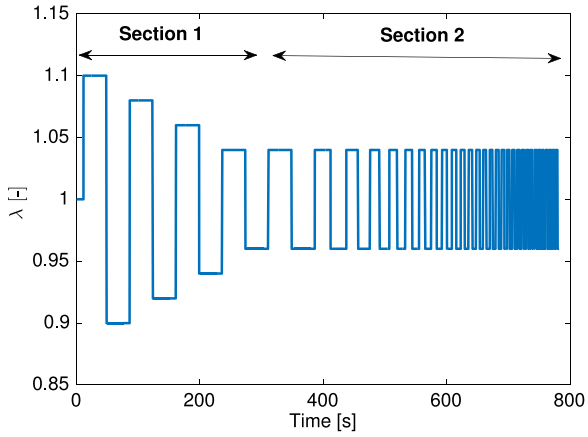


**Fig. 13.** Commanded air–fuel ratio profile used for parameter identification.

### 5.1. Lambda profile for model identification

The experiment designed for parameter identification, inspired by Kiwitz et al. (2012), commands a specific air–fuel ratio profile to the engine. The commanded lambda profile is depicted in Fig. 13. The first section consists of square wave centered around the stoichiometric value with step changes of different amplitude, from 10% down to 4%. The goal is to excite the TWC system with different concentrations of reducing and oxidizing species at the inlet. In Fig. 14, lambda behavior at the pre, mid and post catalyst locations are shown. As expected, the absorption and depletion time of the TWC depends on the concentrations of the incoming oxidizing and reducing species, i.e., it depends on the magnitude of the air–fuel ratio step change. The lower the magnitude of the lambda step change (lower concentrations of oxidizing/reducing species at the inlet), the longer the lambda mid and post plateau around stoichiometry.

The second section of the lambda identification profile consists of constant amplitude lambda step changes (4%) of increasing frequency. Section 2 of the input profile forces the system to remain at an intermediate oxygen storage level, i.e., when the frequency of the step change is high enough, the TWC does not have time to be either completely filled or depleted of oxygen. Thus, the mid and post lambda measurements never match the pre-catalyst value (see Fig. 14). This condition reflects real-world TWC operation where the converter is maintained at an intermediate oxygen storage level, so it can readily compensate for either lean or rich air–fuel ratio disturbances, avoiding CO and $NO_x$ breakthrough at the vehicle tailpipe.

Engine speed and load are kept constant while the lambda profile is commanded, resulting in a nearly constant exhaust temperature and flow rate. The parameters listed in Table 3 describe the dependence of the reaction rates and Gibbs energy on catalyst temperature. In order to obtain a well posed identification problem where the roles of the pre-exponential factors $A_i$ can be separated from the effects of the activation energies $E_i$ and $a$, $b$, and $c$, for a univocal identification, the experiment described is repeated over a wide range of engine operating points with each differently aged TWC. In Table 4, the engine operating points tested are summarized.

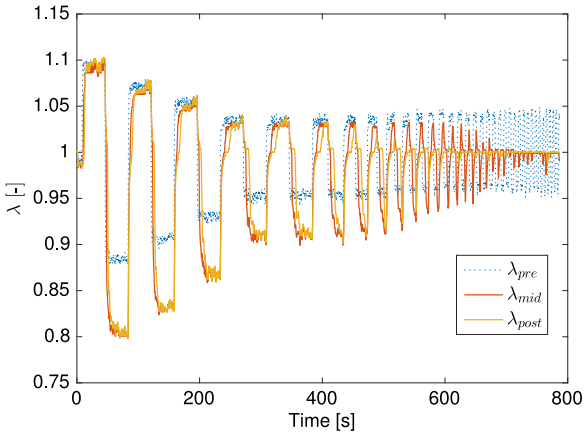


**Fig. 14.** Lambda sensors' response to the identification profile depicted in Fig. 13 on the Mid Life catalyst.

**Table 4**
Engine operating points tested.

| Test | Engine speed [rpm] | $\dot{m}_{exh}$ [g/s] | $T_{exh}$ [°C] |
|---|---|---|---|
| 1 | 1200 | 5.1 | 344 |
| 2 | 1500 | 7.2 | 386 |
| 3 | 1800 | 8.8 | 430 |
| 4 | 2200 | 11.8 | 505 |
| 5 | 2700 | 17.4 | 550 |
| 6 | 3200 | 23.4 | 630 |

To study the variation of total oxygen storage capacity over the operating points tested, a different value for the parameter $OSC$ is identified at each operating point while all other parameters from Table 3 are kept constant. Identification of the reaction rate constants is carried out on the Mid-life catalyst because it is assumed to best reflect the average TWC behavior throughout the whole life cycle.

### 5.2. Parameters optimization

Parameter identification finds the optimal set of parameters that minimizes the error between the simulated lambda at the sensor locations and the actual measured lambda values. As a first step, only the parameters relative to the Brick 1 are found by minimizing the cost function $J$. Defining the parameters vector $\vartheta$ as:

$$\vartheta = \begin{bmatrix} A_1 & A_2 & E_1 & E_2 & a & b & c \end{bmatrix} \tag{23}$$

the cost function is the Root Mean Square (RMS) error evaluated on the normalized air/fuel ratio at the mid location

$$J(\vartheta) = \sqrt{\frac{1}{N_{sample}} \sum_{k=1}^{N_{sample}} (\lambda_{mid_{sim}}(\vartheta, k) - \lambda_{mid_{meas}}(k))^2 \cdot w(k)} \tag{24}$$

where $w(k)$ is a factor that weights the importance of some sections of the identification dataset during the identification process. For example, in Fig. 14, at steady state with rich inlet conditions, the mid and post lambda sensors read substantially richer than the pre-TWC lambda. This is not an effect of the oxygen dynamics in the converter, but reflects the cross-sensitivity of the measured lambda response to the presence of reactive exhaust species. This sensor distortion is well known in literature and is caused by the water-gas shift and steam reforming reactions occurring in the catalyst that have hydrogen as a product. Hydrogen is known to influence lambda sensor measurements due to its high diffusivity in the lambda sensor compared to the other chemical species (Germann, Taglaiferri, & Geering, 1996). To prevent this sensor

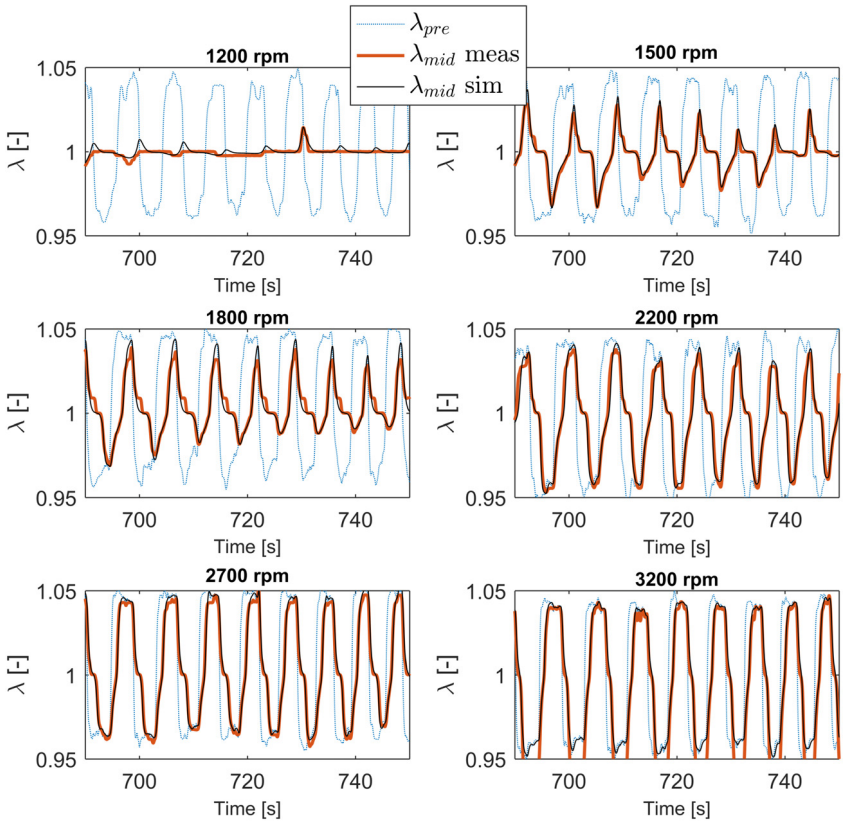


**Fig. 15.** Comparison between the model simulation and the experimental results with the identified parameters on the Mid Life catalyst. Results are presented for each operating point listed in Table 4.

distortion from significantly affecting the cost function in Eq. (24), $w(k)$ is set to zero every time this distortion is detected in the dataset.

The operating points tested span a wide range of exhaust temperatures. As such, the following cumulative cost function comprehensive of all the operating points ($N_{tests} = 6$ as the number of tests performed) is used:

$$J = \sum_{i=1}^{N_{tests}} (J(\vartheta)_i) \tag{25}$$

where $J(\vartheta)_i$ is the RMS error evaluated for the $i$th operating point tested. It is worth noting that, even if the datasets are of different lengths, they still have the same weight on Eq. (25), since the RMS definition in Eq. (24) includes a normalization with respect to the total number of samples $N_{sample}$ in the dataset.

The simultaneous identification of eight parameters represents an optimization problem with a very wide search space. With the cost function (25), a Particle Swarm Optimization (PSO) algorithm was utilized because it has shown good performance in optimization problems with wide search areas despite its simple structure (Ebbesen, Kiwitz, & Guzzella, 2012). The Matlab implementation of the PSO algorithm presented in Ebbesen et al. (2012) is used in this work.

The parameter values determined through the optimization process are listed in Table 3. Fig. 15 compares the performance of the simulation utilizing the identified parameters with the experimental results at each operating point and focusing on Section 2 of the identification profile. The model is proven accurate for all operating points with an RMS error below 3%. Fig. 15 also illustrates that the identified model accurately captures physical trends. For example, increasing the engine speed while utilizing the same commanded lambda disturbance results in a simultaneous increase in $T_{exh}$ and $\dot{m}_{exh}$, which makes the oxygen filling and depletion phases quicker. As a consequence, deviations of lambda mid from the stoichiometric condition become increasingly more evident at high engine speeds.

The parameters of Brick 2 are identified with the same procedure. The estimation of the exhaust species concentrations shown in Fig. 8 is only valid if lambda is measured downstream of the engine and upstream of any catalytic device. For this reason, the estimation of CO, $CO_2$ and $O_2$ downstream of the first brick performed with the Brick 1 model are used as inputs to the second brick model. The lambda simulation $\lambda_{post_{sim}}$ and measurement $\lambda_{post_{meas}}$ downstream the catalyst are then used to compute the cost function presented in Eq. (24). The identified parameters for the second brick are listed in Table 3.

In addition, a sensitivity study of model performance with respect to the number of computational cells has been performed for both the thermal and oxygen storage models. The values of some identified parameters may depend on the number of computational cells utilized during the identification procedure. In order to perform a meaningful and fair comparison, a new parameter identification is performed. In Fig. 16, normalized model error is presented versus the number of computational cells used for the simulation. Fig. 16 shows that using more than 10 cells does not lead to any significant thermal model accuracy improvement. The oxygen storage model experiences no significant improvement when more than three cells are used.

The sensitivity analysis also shows that the choice of the physics-based models, describing both the thermal and the oxygen storage dynamics, enables superior prediction of TWC dynamics relative to simpler empirical models. In fact, when a single computational cell is used, the models are condensed to a lumped input–output formulation, more suited for real-time estimation because of the low computational demand. However, in this lumped formulation, the prediction error for both the oxygen storage and temperature models increases to more than 20% and accuracy would be compromised. This result is in line with other works, Auckenthaler (2005) and Tomforde et al. (2013), where three computational nodes are chosen to describe the oxygen storage dynamics. Additionally, the thermal model performs well with

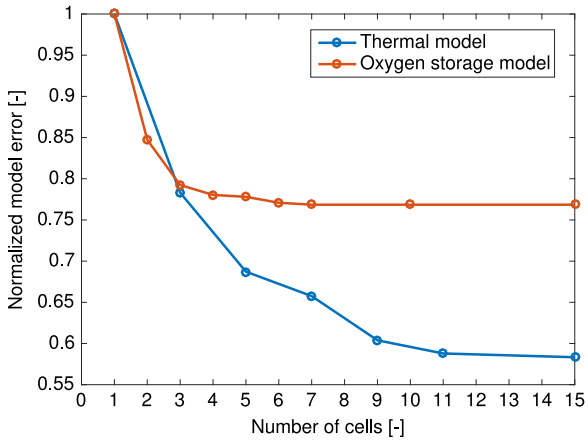


**Fig. 16.** Normalized error for the oxygen storage and thermal models as a function of computational cells. The model error is normalized with respect to values obtained with a single cell-model. The Mid Life catalyst was used in the study reported in this figure.

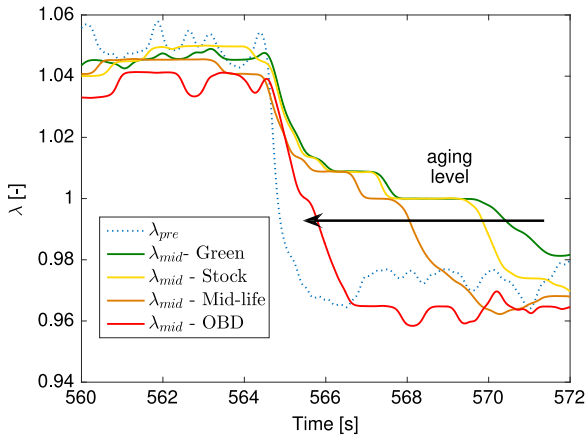


**Fig. 17.** Response of the catalysts listed in Table 2 to a lean-to-rich air–fuel ratio step change.

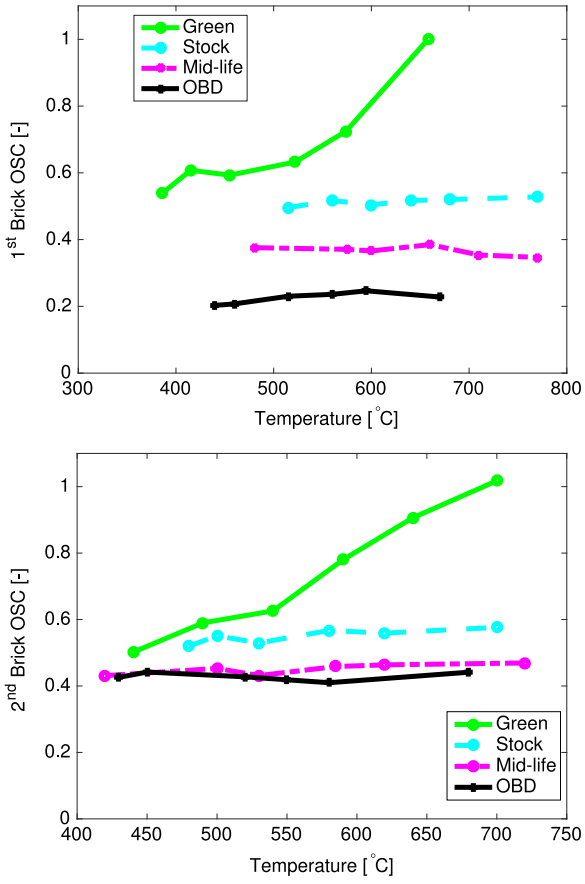


**Fig. 18.** Normalized oxygen storage capacity (OSC) for Brick 1 (upper plot) and Brick 2 (lower plot) resulting from the identification procedure performed on the operating points listed in Table 4 for each catalyst in Table 2.

three cells with the exception of the large temperature gradients experienced during initial TWC warm-up. Because the temperature trends experienced during TWC warm-up apply only during a minimal amount of vehicle operation, both the oxygen storage and thermal models are discretized to three cells to ease computational burden.

## 6. Aging study

A crucial objective of this work is the inclusion of converter aging effects within the TWC model. Previous studies have demonstrated that the total TWC oxygen storage capacity decreases with increased converter utilization (Lambrou, Costa, Christou, & Efstathiou, 2004). Such a trend is also suggested by the mid catalyst lambda responses, shown in Fig. 17, when TWC of different ages (listed in Table 2) are considered.

Fig. 17 shows how the length of the $\lambda_{mid}$ stoichiometric plateau, in response to a step change in TWC $\lambda_{pre}$, consistently decreases with increasing TWC age. This indicates a shorter depletion phase due to the lower amount of oxygen stored in the converter prior to the step change. To investigate the TWC age dependence to model parameters, the identification procedure described in Section 5 is repeated for the Green, Stock, and OBD aged catalysts under the assumption that aging only affects the oxygen storage capacity. The Arrhenius and Gibbs parameters identified for the Mid life catalyst, listed in Table 3, have been used for the other catalyst ages and only the OSC is left free to vary for each catalyst at each operating point.

In Fig. 18, the identified oxygen storage capacities are plotted as a function of the catalyst temperature for all the catalyst ages considered. The model parameter OSC is strongly influenced by the aging level of the converter. Furthermore, the results show that only the Green catalyst oxygen storage capacity is sensitive to the operating point tested. The $OSC$ identified for the last two operating points are substantially higher than the others. This is a product of the simplified reaction mechanism selected for this investigation and the use of Mid life TWC Arrhenius and Gibbs parameters during the OSC identification. The Green TWC appears to experience additional reactivity at elevated temperatures not captured by the mechanism when utilizing Mid life reactivity parameters. For the other three catalyst ages tested, the identified OSC value is insensitive to operating condition, indicating that the simplified reaction mechanism and temperature dependent reaction kinetics using Mid life parameters accurately depict the functionality of the catalyst.

This result is in apparent contrast with some other studies, e.g. the work of Lambrou et al. (2004), where the capacity is shown to increase with temperature approximately 50% for all the aging levels tested. In Lambrou et al. (2004), in contrast to this work, a transient flow system is utilized with the capability to independently vary gas temperature, flow rate, and inlet concentrations. With those capabilities, the oxidizing and reducing species concentrations are tracked upstream and downstream of the catalyst during the converter filling and depletion phases for different gas temperatures at a constant gas flow rate. The capacity identification described in Section 5 minimizes model error with respect the experimental data. For this reason, the capacity value identified is strictly related to the model considered and its simplifications. Therefore some phenomenon that are neglected in the model, like radial mass transport, can influence the capacity calculation especially at elevated temperatures and flow rates.

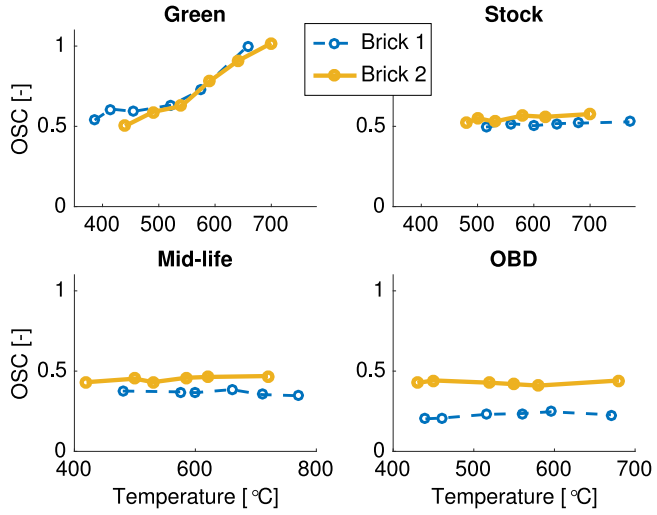


**Fig. 19.** Comparison between the normalized oxygen storage capacity (OSC) for Brick 1 and Brick 2 across TWC aging stages.

The results obtained are of great importance from a control and diagnostic perspective. The fact that TWC aging effects can be lumped within a single model parameter, OSC, which remains constant over the operating range for any one catalyst age, greatly simplifies the design of a model based control strategy. Such a control strategy relies only on the online identification and adaptation of a single parameter.

The same procedure was conducted for the second brick and the identified capacity values are presented in Fig. 18.

Results with the second TWC brick are similar to the first: only the Green catalyst OSC exhibits sensitivity to operating conditions, while for the other catalysts, the capacity can be considered constant over the operating range tested. Note that the capacity values for the Mid-life catalyst are very close to that of the OBD aged catalyst. This is a reasonable result since the Mid-life and OBD aged second bricks underwent a similar aging process (thermal aging cycle) while the first brick for the OBD aged catalyst underwent a confidential process to forcibly simulate a brick which would flag an OBD failure.

In Fig. 19, the identified capacities for Brick 1 and Brick 2 are compared. For the Green catalyst, the two bricks present similar oxygen storage capacities while for the other catalyst ages the first brick exhibits reduced OSC. Furthermore, as the catalyst ages, the difference between the Brick 1 and Brick 2 OSC values increases.

The uneven aging of the two bricks depends on the air–fuel ratio control strategy implemented at the first brick of the partial volume catalyst configuration, aiming to regulate the air–fuel ratio at the mid location at the unity, e.g. $\lambda = 1$. The second brick is used as a "safety oxygen buffer" acting only in the case of breakthrough after the first brick.

## 7. Model validation

The objective of this work is to develop a thermal-oxygen storage-aging TWC model that can be used to design a real time TWC control strategy for fuel saving and TWC health monitoring. It is imperative that the model reflects the system behavior during real driving conditions. Therefore, the model has been validated over the Federal Test Procedure (FTP) drive cycle. From Fig. 20, the performance of the model can be evaluated over the transient section of the FTP cycle. Values of measured and simulated $\lambda_{mid}$ are presented with the model inputs $\dot{m}_{exh}$, $\lambda_{pre}$, $T_{exh}$ and the relative oxygen storage estimation $\phi$. The estimated catalyst brick temperature is also plotted together with the experimental measurements. The test was performed with the default air–fuel ratio control implemented in the vehicle ECU. Fig. 20 exhibits a qualitative evaluation of the oxygen storage estimation accuracy. The model is able to predict with satisfactory accuracy (error is kept below 2%) the lambda measurements. Specifically, the model predicts all the $\lambda_{mid}$ deviations from the stoichiometric condition that are associated with pollutant breakthrough downstream of the first brick.

Fig. 21 illustrates another section of the FTP. In this region, the model is not able to completely and accurately estimate the dynamics of the $\lambda_{mid}$ deviations under pronounced rich conditions. This is not due to an incorrect estimation of the oxygen storage but to the experimental sensor distortion mentioned in Section 5. From an oxygen storage

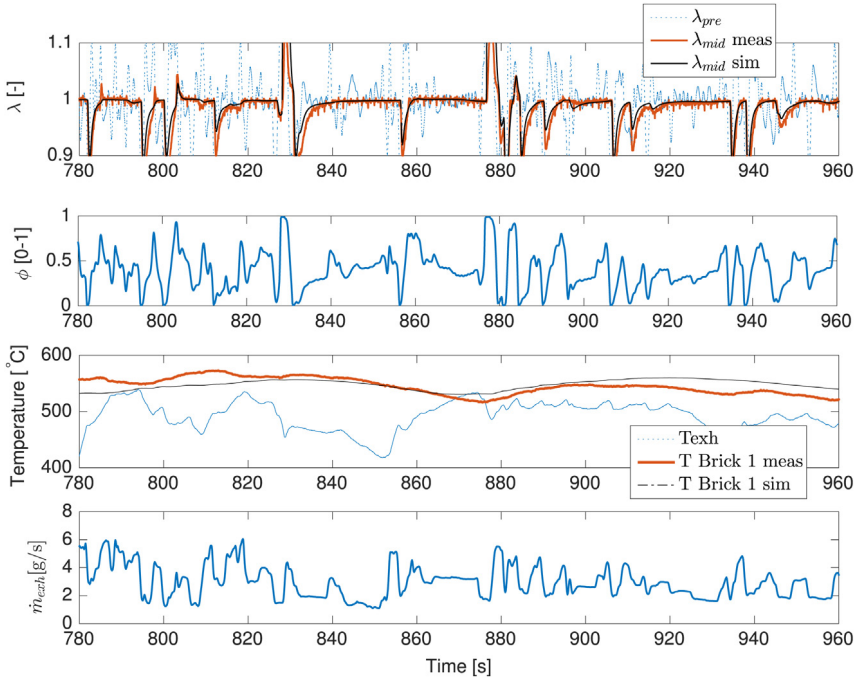


**Fig. 20.** Evaluation of the model performance over the Federal Test Procedure (FTP) (Mid Life catalyst). $\phi$ is the average value of relative oxygen storage level evaluated with 20 spatial discretization cells.

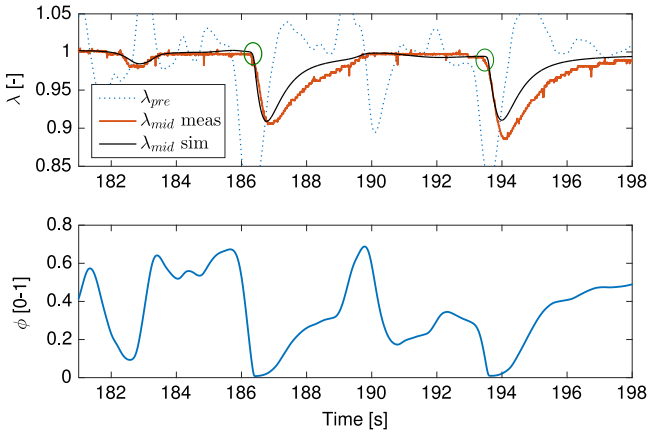


**Fig. 21.** Evaluation of the model performance over the Federal Test procedure FTP (Mid Life catalyst). $\phi$ is the average value of relative oxygen storage level evaluated with 20 spatial discretization cells.

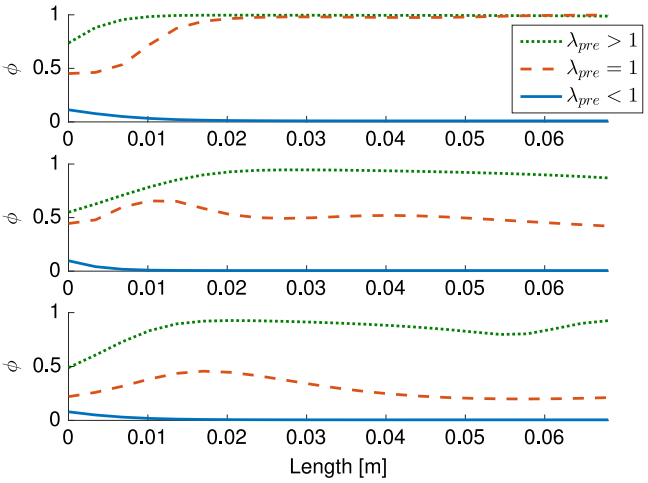


**Fig. 23.** Evaluation of the relative oxygen storage level inside the catalyst along the flow axis for different gas mixture conditions over the FTP cycle analyzed in Fig. 22. The catalyst length has been discretized into 20 cells.

perspective, it is important that the model is able to capture the exact instant that lambda deviates from stoichiometry because these deviations indicate that the converter is nearly almost either full or empty. The circled areas in Fig. 21 indicate when lambda starts to deviate from stoichiometry. The figure also shows that the model predicts the phasing of $\lambda_{mid}$ deviations well, indirectly providing an accurate oxygen storage estimation.

In Fig. 22, simulations of $\lambda_{mid}$ are compared with measurements over the transient FTP section for the Green, Stock, Mid-life and OBD aged catalysts. As identified in Section 6, the model is able to predict, with accuracy, the air–fuel ratio at the mid location for catalysts of various ages. Note that the model accurately predicts an increased number of lambda deviations from the stoichiometric condition for TWC of greater age. With increased age, the TWC's ability to compensate for transient oscillations in pre-catalyst lambda deteriorates because of the reduced the total oxygen storage capacity.

Fig. 23 illustrates an analysis of the relative oxygen storage inside the catalyst along the flow dimension utilizing the model proposed herein. For each catalyst, three different scenarios have been considered, when the normalized air/fuel ratio at the inlet location $\lambda_{pre}$ is at the stoichiometric value and when the gas mixture is either rich or lean.

For all the catalysts, the stored oxygen increases through the converter when $\lambda_{pre} > 1$, while approaches the minimum value when there is not enough oxygen in gas phase. For $\lambda_{pre} = 1$, the catalyst is influenced by the initial conditions and the profiles are not comparable.

Accordingly to the catalyst age, the oxygen stored in the converter decreases. This property is evident along the main dimension: when the exhaust gas is lean, the fresh catalyst quickly stores the oxygen and $\phi$ reaches the maximum value almost in all the catalysts; on the contrary, the more aged the catalyst is, the slower the rate of storage becomes and, with respect to the catalyst length, the last spots of Cerium oxidize later.

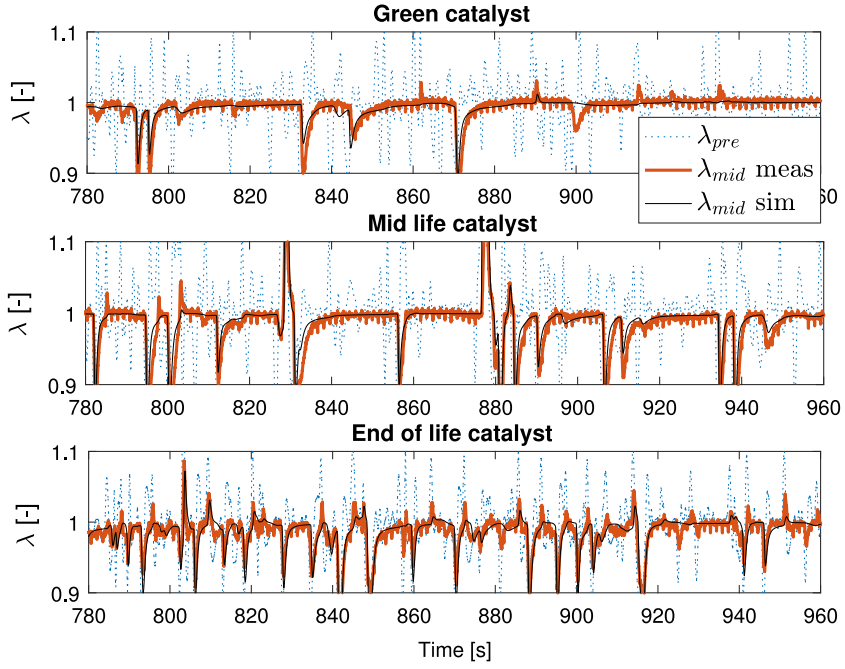


**Fig. 22.** Evaluation of the model performance over the FTP cycle for the Green, the Stock, the Mid Life and the OBD catalysts.

## 8. Conclusions

In this paper, a coupled physics-based thermal-oxygen storage model for TWC was developed and experimentally validated. In addition, TWC aging was experimentally characterized. An aging signature has been found, in the form of lumped aging parameter, OSC. The overall thermal-oxygen level-age model will be included in an optimization-based control framework able to predict and control both $\lambda_{mid}$ and OSC. Ultimately, an integrated model-based control strategy for minimizing fuel consumption and emissions, and monitoring TWC health throughout the TWC life cycle will be designed exploiting the model developed in this paper. This is the subject of ongoing research.

## Acknowledgment

The authors greatly acknowledge the financial support from FCA US LLC (Auburn Hills, MI 48326 USA), under which this work was conducted.

## References

Auckenthaler, T. S. (2005). Modelling and control of three-way catalytic converters. Ph.D. disseration, Technische Wissenschaften, Eidgenössische Technische Hochschule ETH Zürich, Nr. 16018, 2005.

Balenovic, M. (2002). Modelling and Model-based Control of a Three-way Catalytic Converter. Ph.D. dissertation, University of Eindhoven.

Bickel, J., Odendall, B., Eigenberger, G., & Nieken, U. (2017). Oxygen storage dominated three-way catalyst modeling for fresh catalysts. *Chemical Engineering Science*, *160*, 34–53.

Brandt, E. P., Wang, Y., & Grizzle, J. W. (2000). Dynamic modeling of a three-way catalyst for SI engine exhaust emission control. *IEEE Transactions on Control Systems Technology*, *8*(5), 767–776.

Bresch-Pietri, D., Leroy, T., & Petit, N. (2013). Control-oriented time-varying input-delayed temperature model for SI engine exhaust catalyst. In *American control conference (ACC), 2013* (pp. 2189–2195). IEEE.

Chen, P., & Wang, J. (2014). Control-oriented model for integrated diesel engine and aftertreatment systems thermal management. *Control Engineering Practice*, *22*, 81–93.

Cioffi, V., Scala, S., & Sepe, E. (2001). Control oriented modeling of the exhaust gas after-treatment system. In *International Workshop on Modelling, Emissions and Control of Automotive Engines*.

Depcik, C., & Assanis, D. (2005). One-dimensional automotive catalyst modeling. *Progress in Energy and Combustion Science*, *31*(4), 308–369.

DTEC, (2011). http://dtec.net.au.

Ebbesen, S., Kiwitz, P., & Guzzella, L. (2012). A generic particle swarm optimization Matlab function. In *American control conference (ACC), 2012* (pp. 1519–1524). IEEE.

EPA, (2011). http://yosemite.epa.gov/opa/admpress.nsf.

Germann, H., Taglaiferri, S., & Geering, H. P. (1996). Differences in pre-and post-converter lambda sensor characteristics. Technical report, SAE Technical Paper.

Guzzella, L., & Onder, C. (2009). *Introduction to modeling and control of internal combustion engine systems*. Springer Science & Business Media.

Jones, J. C. P., Roberts, J. B., Bernard, P., & Jackson, R. A. (2000). A simplified model for the dynamics of a three-way catalytic converter. Technical report, SAE Technical Paper 2000-01-0652.

Kang, S. B., Han, S. J., Nam, I.-S., Cho, B. K., Kim, C. H., & Oh, S. H. (2014). Detailed reaction kinetics for double-layered Pd/Rh bimetallic TWC monolith catalyst. *Chemical Engineering Journal*, *241*, 273–287.

Katare, S. R., Patterson, J. E., & Laing, P. M. (2007). Diesel aftertreatment modeling: A systems approach to NO x control. *Industrial and Engineering Chemistry Research*, *46*(8), 2445–2454.

Kim, G. (1982). Ceria-promoted three-way catalysts for auto exhaust emission control. *Industrial Engineering Chemistry Production Research Development*, *21*, 267–274.

Kiwitz, P., Onder, C., & Guzzella, L. (2012). Control-oriented modeling of a three-way catalytic converter with observation of the relative oxygen level profile. *Journal of Process Control*, *22*(6), 984–994.

Kumar, P., Makki, I., Kerns, J., Grigoriadis, K., Franchek, M., & Balakotaiah, V. (2012). A low-dimensional model for describing the oxygen storage capacity and transient behavior of a three-way catalytic converter. *Chemical Engineering Science*, *73*, 373–387.

Lambrou, P., Costa, C., Christou, S., & Efstathiou, A. (2004). Dynamics of oxygen storage and release on commercial aged Pd-Rh three-way catalysts and their characterization by transient experiments. *Applied Catalysis B: Environmental*, *54*(4), 237–250.

Lepreux, O., Creff, Y., & Petit, N. (2012). Model-based temperature control of a diesel oxidation catalyst. *Journal of Process Control*, *22*(1), 41–50.

LeVeque, R. J. (2007). *Finite difference methods for ordinary and partial differential equations: steady-state and time-dependent problems, Vol. 98*. Siam.

Möller, R., Votsmeier, M., Onder, C., Guzzella, L., & Gieshoff, J. (2009). Is oxygen storage in three-way catalysts an equilibrium controlled process? *Applied Catalysis B: Environmental*, *91*(1), 30–38.

Montenegro, G., & Onorati, A. (2009). 1D thermo-fluid dynamic modeling of reacting flows inside three-way catalytic converters. Technical report, SAE Technical Paper 2009-01-1510.

Nicolin, P., Rose, D., Kunath, F., & Boger, T. (2015). Modeling of the soot oxidation in gasoline particulate filters. *SAE International Journal of Engines*, *8*(2015-01-1048).

Oh, S. H., & Cavendish, J. C. (1982). Transients of monolithic catalytic converters. Response to step changes in feedstream temperature as related to controlling automobile emissions. *Industrial & Engineering Chemistry Product Research and Development*, *21*(1), 29–37.

Sabatini, S., Kil, I., Dekar, J., Hamilton, T., Wuttke, J., & Smith, M. (2016). Characterization of aging effect on three way catalyst oxygen storage dynamics. SAE Technical Paper 2016-01-0971.

Sabatini, S., Kil, I., Dekar, J., Hamilton, T., Wuttke, J., & Smith, M., and Onori, S. (2015). A new semi-empirical temperature model for the three way catalytic converter. In *IFAC Workshop on Engine and Powertrain Control, Simulation and Modeling*.

Shamim, T., Shen, H., Sengupta, S., Son, S., & Adamczyk, A. (2002). A comprehensive model to predict three-way catalytic converter performance. *Journal of Engineering for Gas Turbines and Power*, *124*(2), 421–428.

Tomforde, M., Drewelow, W., Duenow, P., Lampe, B., & Schultalbers, M. (2013). A post-catalyst control strategy based on oxygen storage dynamics.

VSCHT, (2011). http://old.vscht.cz/monolith/.

Zhu, G., Wang, J., Sun, Z., & Chen, X. (2015). Tutorial of model-based powertrain and aftertreatment system control design and implementation. In *American control conference (ACC), 2015* (pp. 2093–2110). IEEE.